

RESEARCH ARTICLE

Open Access



# Radix puerariae extracts ameliorate paraquat-induced pulmonary fibrosis by attenuating follistatin-like 1 and nuclear factor erythroid 2p45-related factor-2 signalling pathways through downregulation of miRNA-21 expression

Ming-wei Liu<sup>1†</sup>, Rong Liu<sup>1†</sup>, Hai-ying Wu<sup>1</sup>, Yi-yun Li<sup>1</sup>, Mei-xian Su<sup>2</sup>, Min-na Dong<sup>1</sup>, Wei Zhang<sup>1\*</sup> and Chuan-yun Qian<sup>1\*</sup>

## Abstract

**Background:** Puerarin, extracted from *Radix puerariae*, was reported to ameliorate airway inflammation, lung injury and lung fibrosis induced by paraquat (PQ) in mice. However, effects of *Radix puerariae* extracts (RPEs) on lung fibrosis or signalling pathways in PQ-induced lung injury have not been well studied. Therefore, the goals of our study were to investigate whether *Radix puerariae* extracts are antifibrotic in a paraquat (PQ) induced lung fibrosis model in mice and to propose possible mechanisms of action of the RPE effects.

**Methods:** We used a long-term exposure model of PQ-induced lung fibrosis in mice to evaluate effects of antioxidant-containing RPE. We examined effects of miR-21 on follistatin-like 1 (Fstl 1) pathways and oxidative stress in the lung. Gene expression levels of miR-21, Fstl 1, transforming growth factor- $\beta$ 1 (TGF- $\beta$ 1), connective tissue growth factor (CTGF), collagen-1 and collagen III were measured by real-time PCR. Protein expression levels of Fstl 1 (FSTL1), heme oxygenase-1 (HO-1), nuclear factor erythroid 2p45-related factor-2 (Nrf2), Smad2/3, p38MAPK, nuclear factor- $\kappa$ B 65 (NF- $\kappa$ B65), and matrix metalloproteinase-9 were detected by western blotting. FSTL1 and  $\alpha$ -smooth muscle actin ( $\alpha$ -SMA) in lung tissue were detected by immunohistochemistry. Malondialdehyde, superoxide dismutase (SOD), reduced (GSH) and oxidised (GSSH) glutathione and reactive oxygen species levels, hydroxyproline and total lung collagen were also determined.

**Results:** Long-term challenge with PQ enhanced miRNA-21 (miR-21), Fstl 1 pathways, oxidative stress and development of fibrotic features in the lungs. RPE reduced features of lung fibrosis by blocking Fstl 1 pathways and oxidative stress through decreased miR-21 expression. This was accompanied by suppression of CTGF, TGF- $\beta$ 1, vascular endothelial growth factor, collagen I, and collagen III. In addition, PQ-induced activation of NF- $\kappa$ B, Nrf2 and  $\alpha$ -SMA were enhanced by puerarin. We also found that puerarin increased HO-1, SOD and GSH levels.

(Continued on next page)

\* Correspondence: zhangwei7222@126.com; qianchuayun@126.com

<sup>†</sup>Equal contributors

<sup>1</sup>Department of Emergency, the First Affiliated Hospital of Kunming Medical University, 295 Xichang Road, Wu Hua District, Kunming 650032, China

Full list of author information is available at the end of the article



(Continued from previous page)

**Conclusions:** These findings demonstrated that RPEs blocked PQ-induced Fstl 1 pathways and oxidative stress by inhibiting miR-21 expression, leading to attenuation of PQ-induced lung fibrosis.

**Keywords:** Lung fibrosis, Radix puerariae extracts, miR-21, Connective tissue growth factor, Nuclear factor erythroid 2p45-related factor-2, Nuclear factor- $\kappa$ B, Oxidative stress, Mice

## Background

Paraquat, (PQ) widely used as an herbicide, is controversial because of the high mortality of PQ exposure, with a typical case fatality of 50–90 % [1]. The major cause of death by PQ poisoning is respiratory failure, a consequence of oxidative injury to the alveolar epithelium [2]. The primary organ system affected by PQ toxicity is the lung, where PQ is accumulated via an active transport process into Clara cells and alveolar type I and type II epithelial cells. Its initial effects are pulmonary oedema, infiltration of inflammatory cells and damage to the alveolar epithelium, followed by the resulting lung fibrosis and respiratory failure [2–4]. The high fatality of PQ is caused by its inherent toxicity and the lack of any effective treatment [2]. Overall mortality remains above 50 % even in intensive care facilities [2].

The traditional Chinese herbal medicine Radix puerariae has been used to treat alcoholism for thousands of years [5, 6]. In a recent report, puerarin, extracted from Radix puerariae, had antioxidant and antithrombotic effects and decreased cell injuries caused by lipid peroxidation by stabilising cell membranes [7–9]. Such findings indicated that puerarin might prevent PQ-induced pulmonary fibrosis.

MicroRNAs (miRNAs) are a class of non-coding small RNAs, 18–22 nucleotides in length, which bind to target genes and suppress their translation and/or induce degradation of the target gene mRNA. miRNA-21 (miR-21) is one of the most important miRNAs upregulated during fibrogenesis in various tissues [10]. TGF- $\beta$ 1 can stimulate miR-21 expression, detected in the liver, heart, kidneys and lungs of mice [10]. miR-21 is upregulated in the lungs of patients with idiopathic pulmonary fibrosis (IPF) and inhibition of miR-21 attenuates lung fibrosis in mice [11, 12].

Follistatin-like 1 (FSTL1, coded by the Fstl 1 gene), an extracellular glycoprotein, was originally cloned from an osteoblastic cell line as a TGF- $\beta$ 1 inducible gene [13]. FSTL1 is highly homologous to follistatin, which is effective against acute lung injury and bleomycin-induced lung fibrosis by blocking activin and TGF- $\beta$  [14]. The physiological function of FSTL1 remains unclear.

TGF- $\beta$ 1 is known to enhance fibrosis by increasing fibroblast growth and collagen deposition and promoting differentiation of fibroblasts into myofibroblasts [15], which

secrete collagen and other extracellular matrix components. CTGF acts as a cofactor with TGF- $\beta$ 1 to induce fibroblasts to become myofibroblasts, leading to collagen deposition and ultimately resulting in organ scarring and fibrosis [16].

Oxidative stress is one important molecular mechanism underlying fibrosis in a variety of organs, including the lungs [17]. The lungs and all other organs express a wide variety of antioxidants to protect them against oxidative stress. These include catalase, GSH, SOD and HO-1. In addition, Nrf2 is a transcription factor regarded as being the “master regulator” of the antioxidant response [17].

In this study, we demonstrated that antioxidants present in a Radix puerariae extract (RPE) could alter pulmonary fibrosis. We also further explored the underlying signalling pathways of these anti-fibrotic effects using long-term PQ exposure in mice as a model system. We found that RPE ameliorated lung fibrosis and blocked reactive oxygen species (ROS)-associated Fstl 1 activation, oxidative stress and inflammatory signalling pathways by downregulating miR-21 expression.

## Methods

### Preparation of RPE

Radix puerariae, the root of *Pueraria lobata* (Willd) Ohwi (Shanghai Leiyunshang Pharmaceutical Co. Ltd., Shanghai, China) was ground, extracted three times with 70 % alcohol for 2 h, concentrated with a vacuum rotary evaporator and freeze-dried. The dried powder was then dissolved in distilled water and filtered. It was chromatographed on a macroporous resin D101 column (11.5 cm  $\times$  85.5 cm) eluted with distilled water followed by 70 % ethanol. The 70 % ethanol eluate was dried with a rotary evaporator and stored in the dark at 4 °C. A yield of 3.89 g RPE was obtained from 100 g of dried Radix puerariae.

### Extraction and analysis of Radix puerariae

The dried powder sample (200 mg) of RPE was extracted with 5 mL methanol for 12 h on a test tube rotator and centrifuged at 2000  $\times$  g for 10 min and the supernatant collected and evaporated in a Speed-Vac sample concentrator (model SPD 111 V, Thermo Savant, LaJolla, CA, USA). For HPLC analysis, extracts were redissolved in HPLC grade methanol and filtered through a nylon filter (0.45  $\mu$ m, National, Salt Lake City, UT, USA). Sample injection volume for HPLC was 20  $\mu$ L. The HPLC system

was equipped with a pump (L2130; Hitachi, Tokyo, Japan), auto sampler (L-2200; Hitachi) and a UV detector (L-2400; Hitachi) controlled with “Lachrome Elite” software (Waters 2487 instrument software).

HPLC separation was performed on a 250 mm × 4 mm C18 reversed-phase column (5 μm, LichroCART; Merck KGaA, Darmstadt, Germany) protected by a guard column of the same material. The HPLC method was as described by Goyal and Ramawat [8] with small modifications. The solvent system was composed of solvent A (0.0025 % trifluoroacetic acid in water) and solvent B (80 % acetonitrile (E. Merck, Mumbai, India) in solvent A). The column was eluted with successive gradients of solvent A and solvent B, with the percent solvent A programmed as follows: 0–2 min, 85 %; 2–5 min, 85 % → 80 %; 5–15 min, 80 % → 50 %; 15–20 min, 50 % → 40 %; 20–30 min, 40 % → 30 %; 30–35 min, 30 % → 20 %; 35–45 min, 20 % → 0 %; 45–48 min, 0 %; 48–50 min, 0 % → 85 %; 50–55 min, 85 %. Separation was performed at a flow rate of 1.0 mL/min and chromatographic peaks at 254 nm were monitored. The compounds were quantified from a calibration curve constructed with standard solutions. To analyse components of RPE, the concentrations of the chemical reference substance standards used

for plotting the calibration curve ranged from 1.0 to 5.0 μg. Each HPLC run was repeated three times.

The HPLC analysis indicated that 100 mg RPE contained 49.4 mg puerarin, 1.3 mg daidzin, and 0.16 mg daidzein, indicating that puerarin was its major component (Fig. 1).

#### Animals

C57BL/6J (B6) mice were purchased from Kunming Medical University Laboratory Animal Center (Kunming, China). All mice were housed in the Animal Care Facility of Kunming Medical University and maintained in a pathogen-free environment. The mice (8–9 week old and weighing 20–30 g) used in the experiment were housed in a vivarium maintained at 23 °C with a 12:12 h light/dark cycle (lights off at 7.00 p.m.). They received a standard laboratory diet and water *ad libitum*. All experiments were approved by the Ethics Committee of Kunming Medical University (Yunnan, China) (Approval number: TCM-2011-041-E17) and performed according to The Guidelines of the Animal Care Committee of Kunming Medical University.

#### In vivo miR-21 knockdown using locked nucleic acid-modified anti-miR-21

Locked nucleic acid (LNA)-modified scrambled or anti-miR-21 oligonucleotides (Exiqon, Woburn, MA, USA) were diluted in saline (5 mg/mL) for administration through intraperitoneal (i.p.) injection (10 mg/kg) at least 30 min before PQ exposure [18].

#### Reagents

PQ aqueous solution (active ingredient content of 200 g/L, product license number: XK13-003-00058) was from Chuandong Agrochemical Co., Ltd, (Guangdong, China). An enhanced chemiluminescence (ECL) kit was from Perkin Elmer Life Sciences, Inc. (Boston, MA, USA). SYBR fluorescence quantitative reverse transcription polymerase chain reaction (PCR) kit was from Takara Company (Tokyo, Japan). TRIzol reagent was from Invitrogen Corporation (Carlsbad, CA, USA), Mouse TGF-β1 and MMP-9 ELISA kits were from Bender Medsystem (Vienna, Austria).

#### Animal treatments

In the first experiment, mice were weighed and randomly divided into five groups (five mice per group) to assess protective effects of puerarin on pulmonary fibrosis. For induction of pulmonary fibrosis, PQ (10 mg/kg) or saline, as a control, was injected i.p. into mice [3]. Group 1 was untreated (or, where indicated, received only saline) and served as the control group; Group 2 received PQ (10 mg/kg) to induce pulmonary fibrosis and served as the “model group”; Group 3 received PQ to induce pulmonary fibrosis

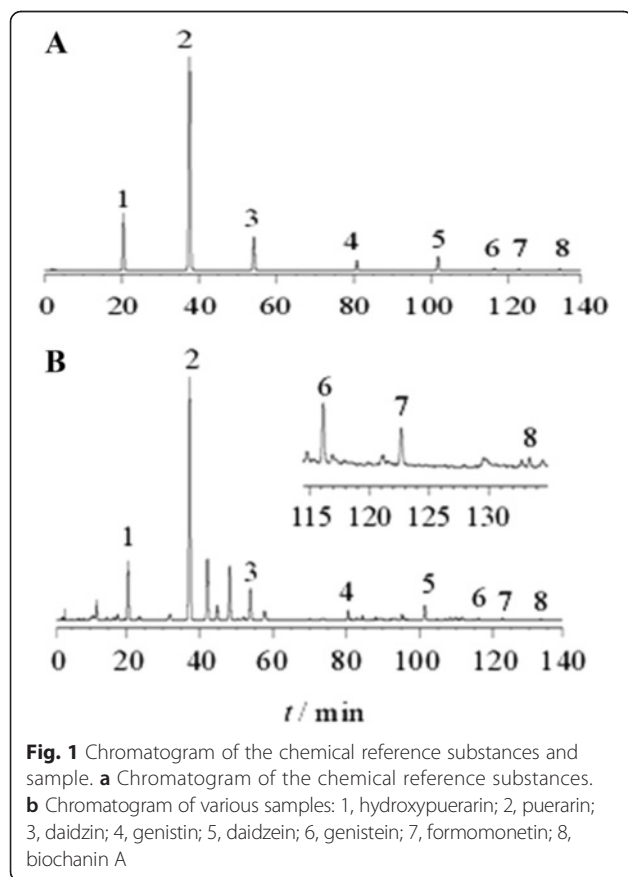


**Table 1** Primer sequences for the genes to validate microarray analysis by real-time-PCR

miRNA-21	F: 5'-TGACATCGCATGGCTGTA-3' R: 5'-GATGCTGGGTAATGTTTGAAT-3'	336 bp
Fstl1	F: 5'-TTATGATGGGCACrGCAAAGAA-3' R: 5'-ACTGCCTTTAGAGAACCAGCC-3'	405 bp
TGF-β1	F: 5'-CAAGAACAAGGCAGACTTATCGC-3' R: 5'-TCTGATTATCTCGACCAGGAAG-3'	418 bp
CTGF	F: 5'-TTCGGTGTACGGTGTACCGCA-3' R: 5'-ACGAACGTCATGCTGCACAGG-3'	359 bp
collagen-1	F: 5'-ACCTGCGTACAGAACGGCCT-3' R: 5'-ACAACACCTTGCCGTTGTCGC-3'	318 bp
Collagen III	F: 5'-GGATCTGCTCTTTCGATGAC-3' R: 5'-GCTGTGGGCATATTGCACAA-3'	276 bp
β-actin	F: 5'-CCTCATGAAGATCCTGACCG-3' R: 5'-ACCGCTCATTGCCGATAGTG-3'	190 bp

and was also treated with RPE at a dose of 30 mg/kg i.p. once per day. On day 14 after PQ injection, mice were killed and lungs harvested. A small portion of each lung was fixed with 10 % formalin and embedded in paraffin for haematoxylin-eosin (HE) and Masson's trichrome staining.

#### Real-time PCR analysis

For RNA isolation, lung tissues were frozen in liquid nitrogen and stored in a  $-80^{\circ}\text{C}$  freezer until use. Total RNA was extracted from frozen lung tissue (left lung) with TRIzol reagent and amplified with a PCR single-step kit (Promega, Madison, WI, USA) according to the manufacturer's instructions. Real-time-PCR was performed with a PTC-200 DNA Engine PCR cycler (Bio-Rad Laboratories, Inc., Hercules, CA, USA). The primers (Table 1) were designed based on published sequences of these genes and synthesised by Invitrogen [19, 20]. PCR was performed in a total volume of 20  $\mu\text{L}$  containing 20 mM Tris-HCl, 50 mM KCl, 1.25 mM  $\text{MgCl}_2$ , 0.2 mM dNTP, 0.5 mM primer, 1 U TaqDNA polymerase and 0.5  $\mu\text{L}$  cDNA. Cycle parameters were as follows:  $95^{\circ}\text{C}$  for 3 min, 25 cycles ( $98^{\circ}\text{C}$  for 30 s,  $60^{\circ}\text{C}$  for 40 s, and  $72^{\circ}\text{C}$  for 60 s) and  $72^{\circ}\text{C}$  for 5 min. Ordinary PCR products were separated on a 2 % agarose gel.  $\beta$ 2-Actin was used as an endogenous control and values for each sample were normalised according to its  $\beta$ 2-actin content. The mRNA expression levels of target genes were calculated using the  $2^{-\Delta\Delta\text{Ct}}$  method [21, 22].

#### Western blotting

Lung homogenates were prepared in lysis buffer (50 mM Tris-HCl, 150 mM NaCl, 1 % NP-40, 0.5 % sodium deoxycholate, 2 mM NaF, 2 mM EDTA, 0.1 % SDS and a protease inhibitor cocktail tablet (Roche Applied Science, Indianapolis, IN, USA). Protein concentrations

were quantified by the BCA method (Pierce Biotechnology, Inc., Rockford, IL, USA). An equal amount of protein (30 mg) from each sample was loaded on respective gel lanes. Samples and pre-stained molecular weight markers (Bio-Rad) were electrophoresed on 12 % Tris-glycine polyacrylamide gels, then protein bands were electrophoretically transferred onto polyvinylidene difluoride (PVDF) membranes (Millipore Corp., Marlborough, MA, USA). Membranes were blocked for 1 h at room temperature with 5 % bovine serum albumin (BSA) and then incubated overnight at  $4^{\circ}\text{C}$  with the following primary antibodies: anti-MMP-9 (Santa Cruz Biotechnology, Dallas, TX, USA), anti-p-p38MAPK (Bio-Rad Laboratories Inc.), anti-NF- $\kappa$ B65 (DAKOCorp, Carpinteria, CA, USA), anti-HO-1 (Cell Signaling, Beverly, MA, USA), anti-Nrf2 (Cell Signaling), anti-FSTL1 (R&D systems, Minneapolis, MN, USA), anti-p-Smad2/3 (Serotec Ltd, Oxford, United Kingdom), anti-TGF- $\beta$ 1 (Sigma, St. Louis, MO, USA), anti-CTGF (Santa Cruz Biotechnology), anti-collagen III (Santa Cruz Biotechnology), anti-collagen-1 (Invitrogen), and anti- $\beta$ -actin (Sigma-Aldrich), each diluted 1:1000 in Tris-buffered saline with Tween-20 (TBST).  $\beta$ -actin blotting served as the control to confirm protein loading. After washing with TBST, membranes were incubated with the corresponding horseradish peroxidase-linked anti-rabbit antibody (Pierce) diluted in TBST (1:20000) for 1 h at room temperature. After further washing with TBST, immunoreactive bands were visualised by enhanced chemiluminescence (ECL) and quantified by densitometry using Bio-Rad Universal Hood and Quantity One software (Bio-Rad). Results were normalised to  $\beta$ -actin levels in the same lanes.

#### Enzyme-linked immunosorbent assay (ELISA)

At 24 h after the last challenge, bronchoalveolar lavage (BAL) fluid was obtained from the anaesthetised mice with 1 mL sterile isotonic saline. Lavage was performed four times and the total volumes pooled for each mouse. Lavage fluid samples were immediately centrifuged at  $2000 \times g$  for 10 min at room temperature and stored at  $-80^{\circ}\text{C}$  until use. TGF- $\beta$ 1 and MMP-9 levels were then assayed with TGF- $\beta$ 1 and MMP-9 ELISA kits according to the manufacturers' instructions.

#### Immunohistochemistry

Immunostaining was performed on lung sections after antigen retrieval using Retrieval A (Zymed, South San Francisco, CA, USA) at  $100^{\circ}\text{C}$  for 20 min and then quenching endogenous peroxidases with 3 %  $\text{H}_2\text{O}_2$ . Sections were blocked with 2 % BSA in PBS followed by staining with primary anti-FSTL1 and  $\alpha$ -SMA at room temperature for 1 h. Sections were then washed. After application of the secondary antibody (Sigma-Aldrich), tissue staining was developed with Vectastain ABC (Vector Labs, Burlingame, CA, USA) and 3,3'-

diaminobenzidine (Vector Labs). With Image Pro Plus image analysis software (Media Cybernetics, Bethesda, MD, USA), FSTL1 and  $\alpha$ -SMA positive staining in lung tissue were determined and each staining intensity was expressed as positive units.

#### Total lung collagen

Total lung collagen was determined by measuring total soluble collagen (Sircol Collagen Assay, Biocolor, Belfast, Northern Ireland). The left lung was homogenised in 5 mL 0.5 M acetic acid containing pepsin (1 mg/10 mg tissue; Sigma-Aldrich) and incubated (24 h, 24 °C, with mixing at 240 rpm). Sircol dye was added (1 mL/100 mL, with mixing for 30 min) and then the sample was centrifuged (12,000  $\times$  g for 12 min). The pellet was resuspended in 1 mL 0.5 M NaOH. The optical density at 540 nm was measured with a spectrophotometer.

#### Measurement of intracellular ROS

ROS were measured as previously described [23]. BAL cells were washed with PBS and incubated for 10 min at room temperature with PBS containing 3.3  $\mu$ M 2',7'-dichlorofluorescein (DCF) diacetate (Molecular Probes, Eugene, OR, USA) to label intracellular ROS. DCF stained cells were analysed by fluorescence-activated cell sorting ( $1 \times 10^4$  cells).

#### SOD activity assay

SOD activity was estimated as described by Kakar et al. [24]. The reaction mixture contained 0.1 mL phenazine methosulphate (186  $\mu$ M) and 1.2 mL sodium pyrophosphate buffer (0.052 mmol, pH 7.0). Lung homogenate was prepared in 10 mL ice-cold lysis buffer (50 mM phosphate buffer with 1 mM Methylene diamine tetraacetic acid (EDTA) per g tissue and centrifuged twice (once at 1500  $\times$  g for 10 min, and the supernatant centrifuged again at 10,000  $\times$  g for 15 min). An aliquot (0.3 mL) of the resulting supernatant was added to the reaction mixture. The enzymatic reaction was initiated by adding 0.2 mL NADH (780  $\mu$ mol) and stopped after 1 min by adding 1 mL glacial acetic acid. The amount of chromogen formed was measured by absorbance at 560 nm. Results are expressed in units/mg protein.

#### Measurement of malondialdehyde (MDA)

Lung tissue homogenates from control and experimental groups were prepared in 0.1 M Tris-HCl buffer (pH 7.4) at 4 °C. The resulting tissue homogenates were used for all biochemical measurements unless otherwise indicated. MDA content was determined by a colorimetric assay with a commercially available kit (Jiancheng Bio-engineering Institute, Nanjing, China) according to the manufacturer's instructions. Briefly, MDA content in the lung was measured according to the thiobarbituric acid

method based on the formation of a red complex when MDA reacted with thiobarbituric acid. The absorbance was spectrophotometrically measured at 532 nm.

#### Measurement of GSH and GSSG in lung tissues

Lung tissues were homogenised with 10 mL ice-cold buffer (50 mM phosphate buffer containing 1 mM EDTA per gram tissue). After centrifugation at 10,000  $\times$  g for 15 min at 4 °C, the supernatants were removed, deproteinated with 7.5  $\mu$ l 5 M KOH per 500  $\mu$ l volume and then stored at -20 °C until assayed. Total GSH and GSSG levels were determined with a GSH Assay Kit (Cayman Chemical Company, Ann Arbor, MI, USA) according to the manufacturer's protocol.

#### Hydroxyproline assay

Collagen content was determined based on hydroxyproline (HYP) levels [25]. Briefly, 10 mg lung tissue was minced in 1 mL 6 M HCl, hydrolysed and then incubated overnight at 120 °C. Five milliliters 0.5 M acetic acid was added and the pH adjusted to between 6.0 and 6.5 with 0.2 M NaOH. Chloramine T solution (1 mL, 0.05 M) was added and the mixture was incubated for 20 min at room temperature. Aldehyde-perchloric acid (1 mL of a 0.5 M solution) was added and the mixture incubated at 60 °C for 15 min. Absorbance was then recorded at 550 nm. Results are expressed as  $\mu$ g/mg wet lung weight with HYP values read from a standard curve.

#### Histopathology

Whole lungs were inflated *in situ* with PBS-buffered formalin (4.5 %, pH 7.0) (Roth, Darmstadt, Germany) and then carefully immersed in more PBS-buffered formalin. Lung tissue samples were paraffin-embedded and 5- $\mu$ m-thick sections were prepared and stained with haematoxylin/eosin (H/E) and Masson's or Elastica-van-Gieson staining. The degree of lung fibrosis was assessed in lung samples as described by Ashcroft and colleagues [26] with a numerical scaling system. In the scaling system, 0 indicates normal lung and eight indicates total fibrous obliteration of the field. Mean lung fibrosis degree, as defined by Ashcroft et al. [26], was calculated from individual scores of ~15 microscopic fields analysed per mouse lung.

#### Statistical analysis

All values were expressed as the means  $\pm$  standard deviation (SD) or means  $\pm$  standard error of the mean (SEM), as indicated in the individual figure legends. A one-way ANOVA followed by the Student-Newman-Keuls test was used to compare the differences among multiple groups. Pulmonary fibrosis scores were compared using nonparametric methods. The significant level was defined by a *P*

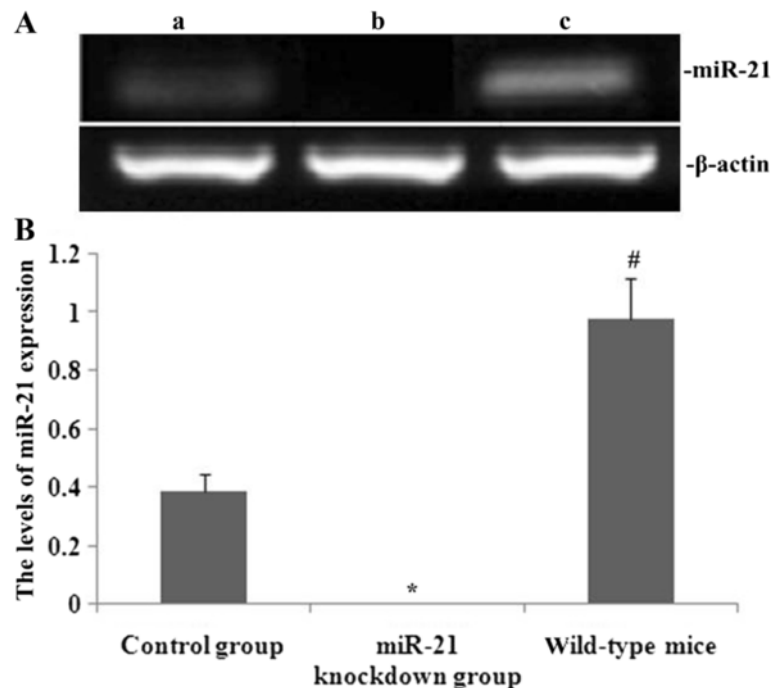


**Fig. 2** Effect of miR-21 knockdown on miR-21 expression in lungs from PQ-treated mice. Groups of mice were treated with PQ for 14 days to induce pulmonary fibrosis. miR-21 expression in pulmonary tissue was determined using real-time PCR. **a** Typical patterns of miR-21 expression as assessed by real-time PCR (a, control (scrambled oligonucleotide) group; b, miR-21 knockdown group; c, wild type group); **b** Statistical analysis of miR-21 expression. Data are means  $\pm$  SD from triplicate experiments. \* $P < 0.05$  vs control group; # $P < 0.05$  vs miR-21 knockdown group

value of 0.05. The SPSS 13.0 software package (SPSS, Inc., Chicago, IL, USA) was used for statistical analyses.

## Results

### Effect of miR-21 knockdown on miR-21 expression in lungs from PQ-treated mice

We investigated effects of miR-21 knockdown on miR-21 expression in lung tissue from mice treated with PQ. Groups of mice were treated with PQ for 14 d to induce pulmonary fibrosis. This pulmonary fibrosis model was established in both miR-21 knockdown and wild-type (WT) mice. miR-21 expression in pulmonary tissue was determined by real-time PCR. As shown in Fig. 2, real-time PCR demonstrated no miR-21 expression in lungs from the miR-21 knockdown mice, that is, those that had been treated with the anti-miR-21 oligonucleotides.

### miR-21 knockdown decreased FSTL1 expression and mitigated PQ-induced pulmonary fibrosis

Western blotting was performed to observe the effect of miR-21 knockdown on FSTL1 protein levels in PQ-induced pulmonary fibrosis. As shown in Fig. 3, after PQ treatment, lung expression of FSTL1 was increased and pulmonary fibrosis exacerbated in miR-21 knockdown and wild-type (WT) mice. However, protein expression of FSTL1 was significantly decreased and pulmonary

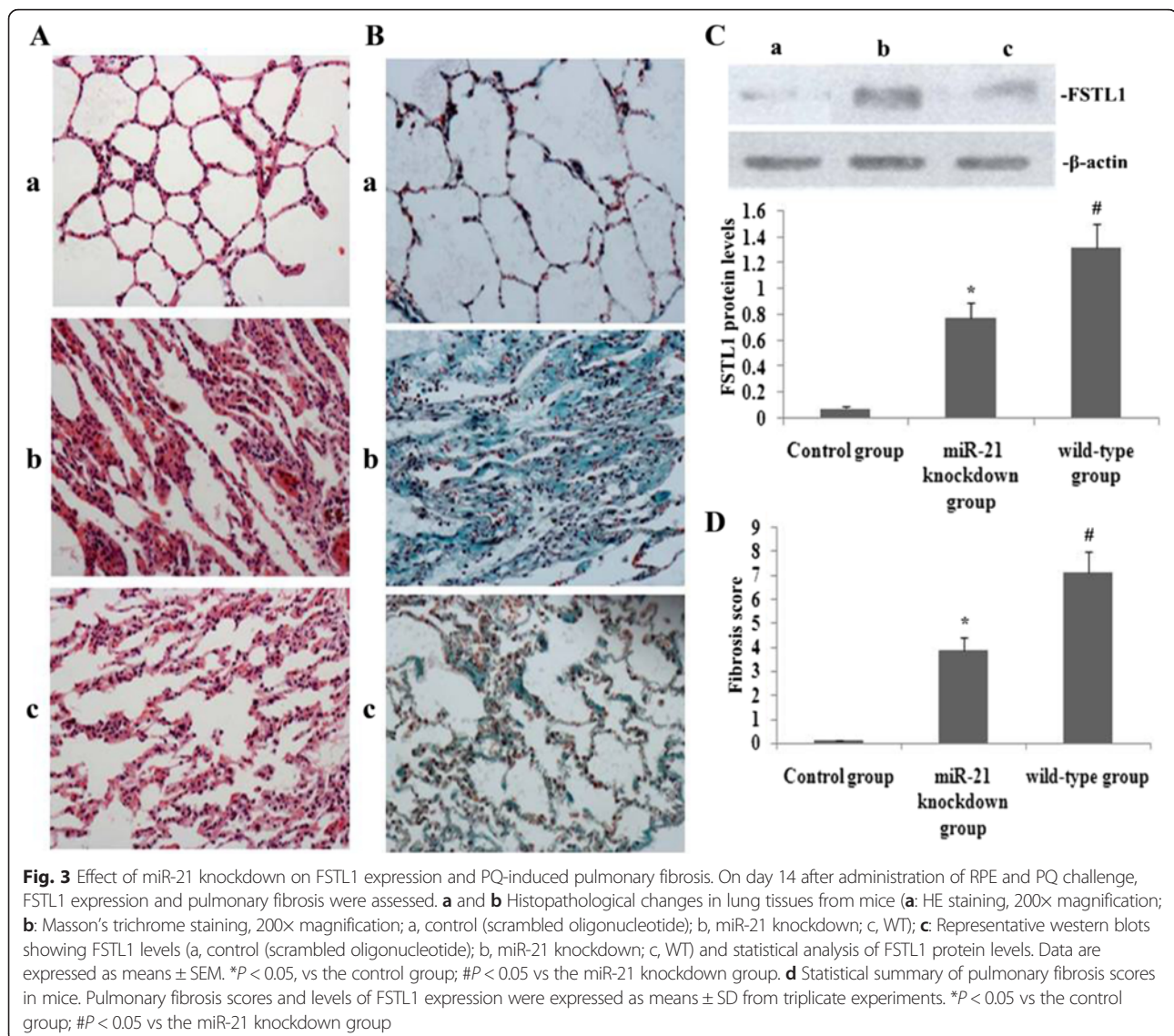
fibrosis was attenuated in the miR-21 knockdown mice, as compared with in WT mice.

### RPE blocked miR-21, FSTL1, p-p38MAPK, NF-kB65, p-Smad2/3 and matrix metalloproteinase 9 (MMP-9) expression in lungs from PQ-treated mice

To assess effects of RPE in PQ-induced lung fibrosis, we measured miR-21 and FSTL1 gene expression with real-time PCR and p-p38MAPK, NF-kB65, p-Smad2/3 and MMP-9 protein expression with western blotting in lung tissue from mice on day 14 after PQ challenge. As shown in Fig. 4, expression levels of miR-21, FSTL1, p-p38MAPK, NF-kB65, p-Smad2/3 and MMP-9 in the lung were increased during PQ-induced pulmonary fibrosis. In mice also treated with RPE, expression of all these genes was significantly decreased.

### RPE treatment downregulated expression of TGF- $\beta$ 1, CTGF, collagen III and collagen I in the lung

To clarify effects of RPE on the expression of TGF- $\beta$ 1, CTGF, collagen III and collagen I genes under challenge by PQ, mRNA and protein expressions of TGF- $\beta$ 1, CTGF, collagen III, and collagen I were measured by real-time PCR and western blotting, respectively. The mRNA and protein expression levels of



TGF- $\beta$ 1, CTGF, collagen III and collagen I in the mouse lung were significantly increased during PQ-induced pulmonary fibrosis ( $P < 0.05$ , Figs. 5, 6). However, these mRNA (Fig. 5) and protein (Fig. 6) expression levels were significantly decreased in mice treated with RPE ( $P < 0.05$ ).

#### RPE treatment increased HO-1 and Nrf2 protein expression in the lung

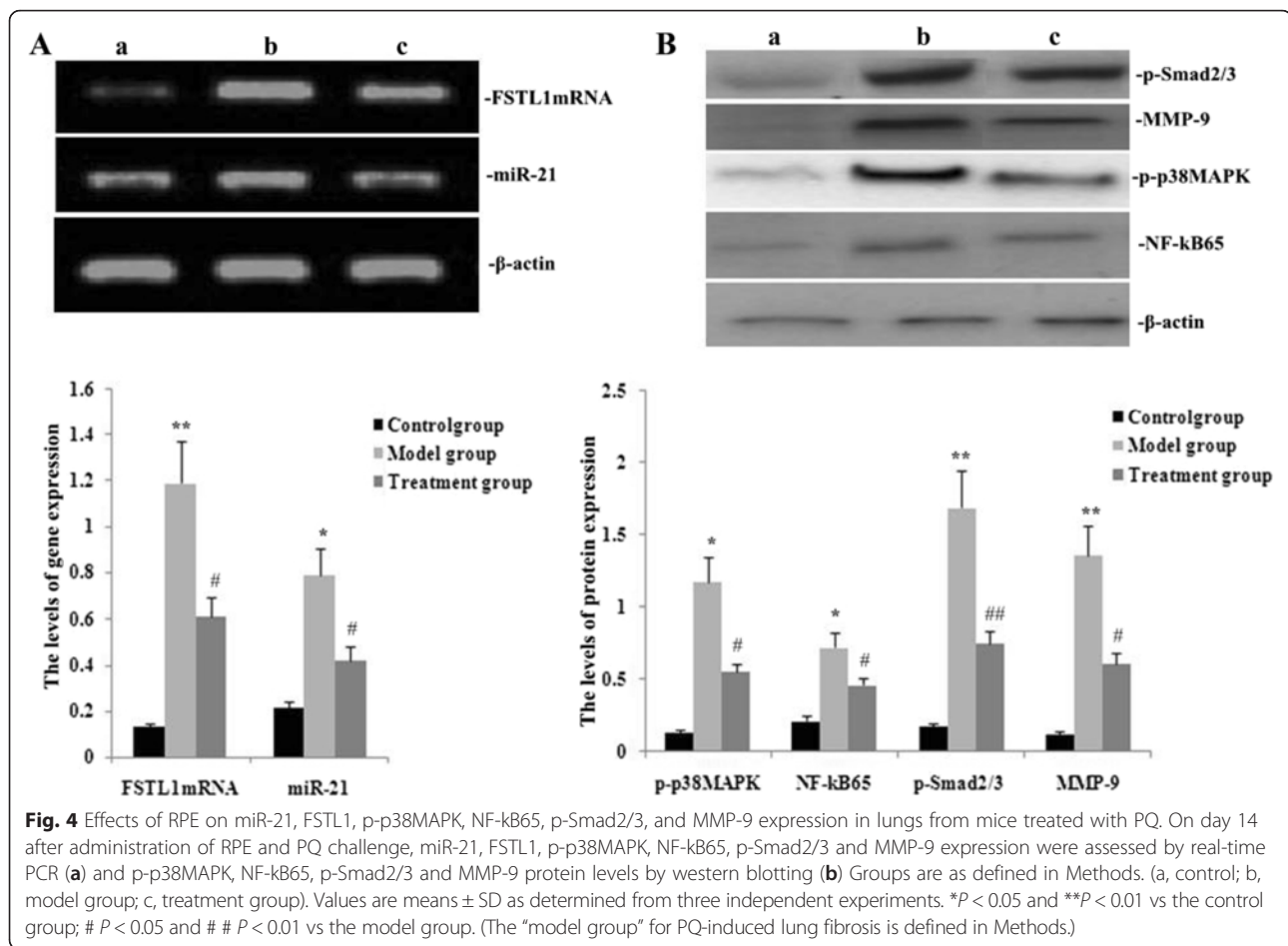
To observe effects of RPE on expression of HO-1 and Nrf2 proteins in the lungs in PQ treated mice, we used western blotting. Protein levels of HO-1 and Nrf2 in the lung were significantly decreased during PQ-induced pulmonary fibrosis but were significantly higher in mice also treated with RPE (Fig. 7).

#### Effects of RPE treatment on FSTL1 and $\alpha$ -SMA staining in lungs from PQ-treated mice

Immunohistochemical analysis was used to determine distribution of FSTL1 and  $\alpha$ -SMA in the mouse lung on day 14 after PQ or saline treatment. Staining for FSTL1 and  $\alpha$ -SMA was localised to alveolar epithelium. The number of cells expressing FSTL1 and  $\alpha$ -SMA was significantly increased during PQ-induced pulmonary fibrosis and this increase was significantly reduced by RPE treatment (Fig. 8).

#### RPE treatment decreased TGF- $\beta$ 1 and MMP-9 levels in BAL from PQ-treated mice

BAL fluids were collected 24 h after PQ treatment to evaluate levels of MMP-9 and TGF- $\beta$ 1. PQ caused



significant pulmonary fibrosis, as indicated by increased BAL concentrations of TGF- $\beta$ 1 and MMP-9. Treatment of mice with RPE reduced the increases in TGF- $\beta$ 1 and MMP-9 levels (Fig. 9).

#### RPE treatment ameliorated oxidative stress

To analyse effects of RPE on oxidative stress, SOD activity and levels of ROS, MDA, GSH and GSSG were determined. As shown in Fig. 10, ROS, MDA and GSSG levels were significantly increased and GSH levels and SOD activity were markedly decreased on day 14 after PQ administration. However, RPE treatment significantly attenuated these indicators of oxidative stress.

#### RPE administration attenuated PQ-induced pulmonary fibrosis

We assessed effects of RPE treatment on PQ-induced pulmonary fibrosis using histological staining. Masson's trichrome and H&E staining revealed significant thickening of alveolar septa and collagen deposition in the lungs on day 14 after PQ administration (Fig. 11a and b). The degree

of PQ-induced pulmonary fibrosis was greatly attenuated in mice also treated with RPE.

Dense fibrosis with prominent collagen deposition was observed in the lungs on day 14 after PQ administration. The degree of dense fibrosis with collagen deposition induced by PQ was greatly attenuated by RPE treatment (Fig. 11a–c). No abnormal alveolar architecture was observed in lungs of the saline-administered control mice.

Next, we assessed the degree of pulmonary fibrosis using a scoring method. In PQ-treated mice, the scores of fibrotic lesions were significantly worse (that is, higher scores) on day 14 after PQ administration compared with those of saline-administered controls (Fig. 11c). However, the scores were significantly improved by RPE administration to PQ-treated mice.

Based on measurements of lung HYP content, we further assessed the degree of pulmonary fibrosis, observing a significant increase on day 14 after PQ administration (Fig. 11c). However, HYP content was significantly lower in PQ-treated mice that had also received RPE (Fig. 11c).

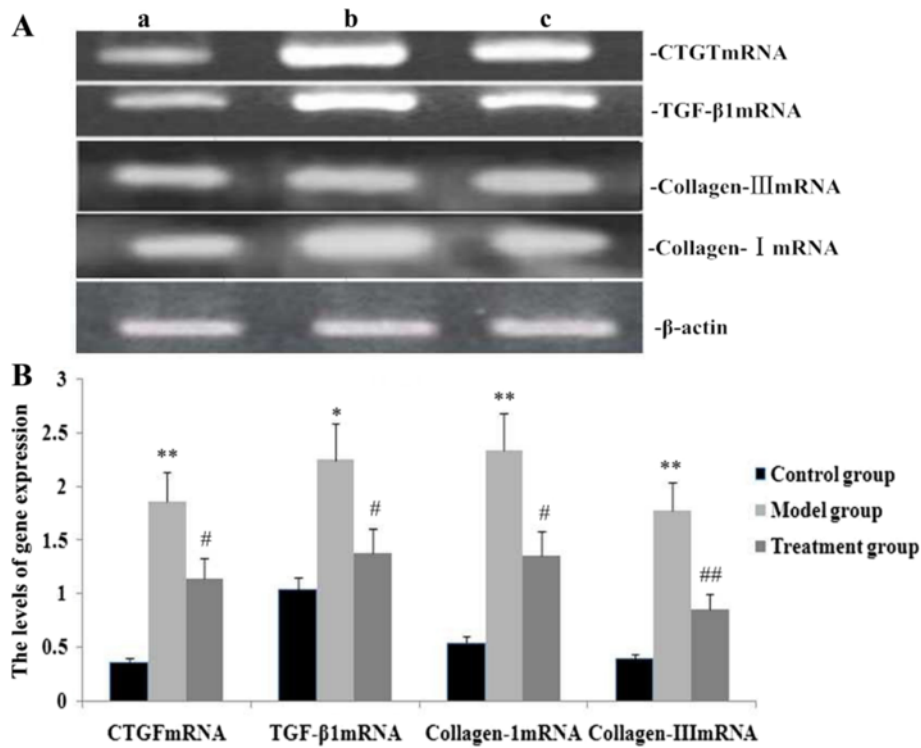


**Fig. 5** Effects of RPE treatment on gene expression of TGF-β1, CTGF, collagen III and collagen I in the lung. **a** Representative real-time PCR showing expression levels of TGF-β1, CTGF, collagen III and collagen I in mice on day 14 after the administration of RPE (a, control group; b, model group; c, treatment group). **b** Statistical summary of the  $2^{-\Delta\Delta Ct}$  analyses on mRNA expression in mice. Data are the means  $\pm$  SD as determined from three independent experiments. \* $P < 0.05$  and \*\* $P < 0.01$  vs the control group; #  $P < 0.05$  and ##  $P < 0.01$  vs the model group

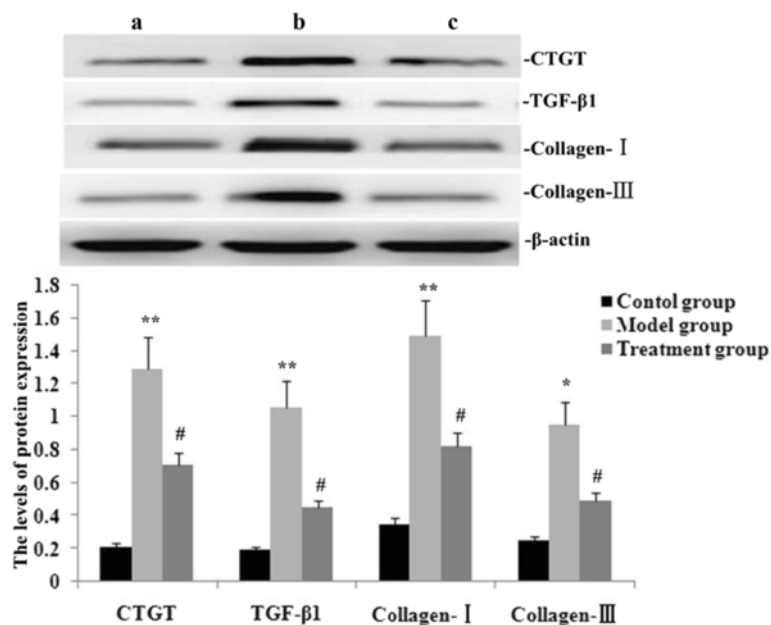


**Fig. 6** Effect of RPE treatment on protein expression of TGF-β1, CTGF, collagen III and collagen I in the lung. **a** Representative western blots showing expression levels of TGF-β1, CTGF, collagen III and collagen I in mice on day 14 after administration of RPE (a, control group; b, model group; c, treatment group). **b** Statistical summary of the densitometric analyses of protein expression in mice. Data are the means  $\pm$  SD as determined from three independent experiments. \* $P < 0.05$  and \*\* $P < 0.01$  vs the control group; #  $P < 0.05$  and ##  $P < 0.01$  vs the model group

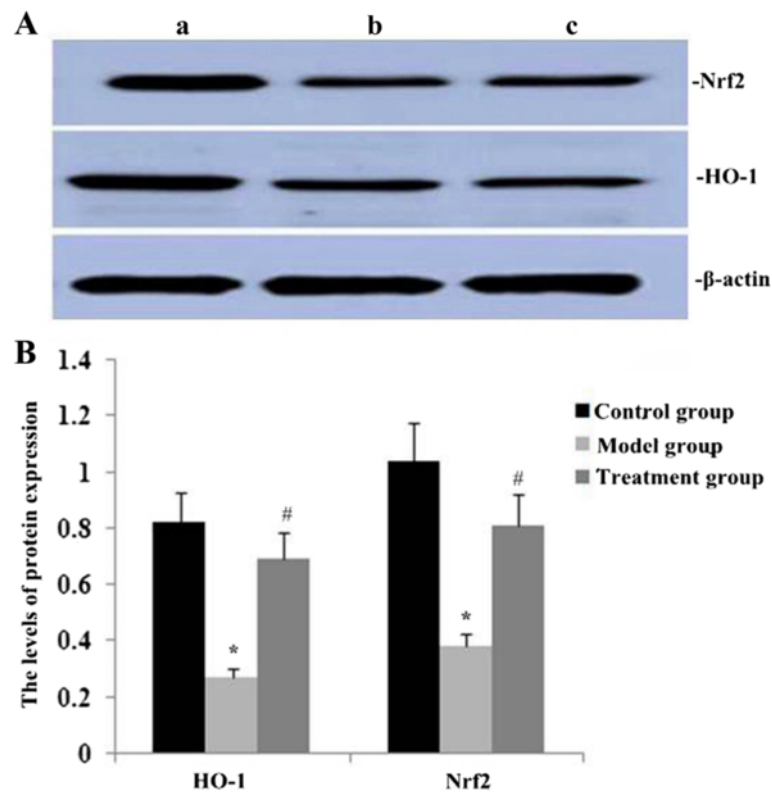


**Fig. 7** Effect of RPE treatment on protein expression of HO-1 and Nrf2 in the lung. **a** Representative western blots showing HO-1 and Nrf2 protein on day 14 after RPE treatment (1, control group; 2, model group; 3, treatment group). **b** Statistical summary of the densitometric analyses of HO-1 and Nrf2 expression. Data are means  $\pm$  SD of three experiments. \* $P < 0.05$  and \*\* $P < 0.01$  vs the control group; ## $P < 0.01$  and # $P < 0.01$  vs the model group

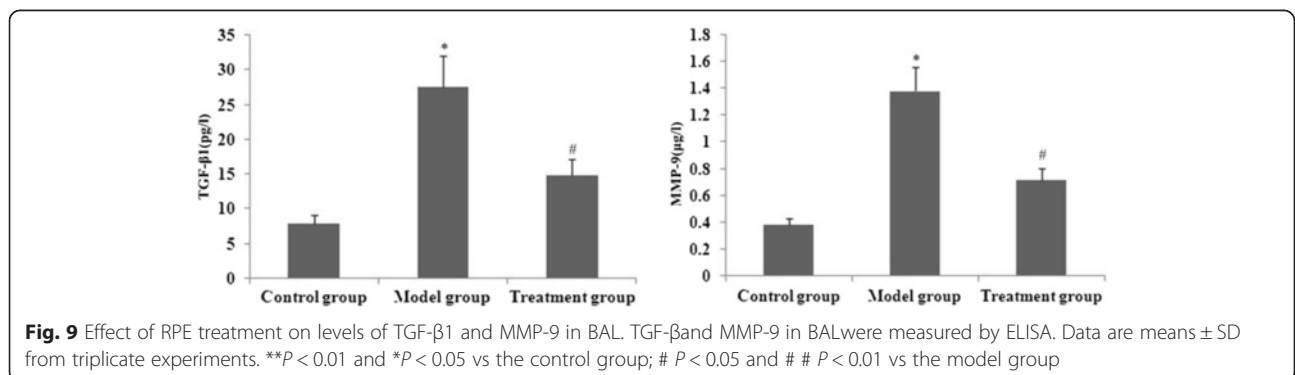
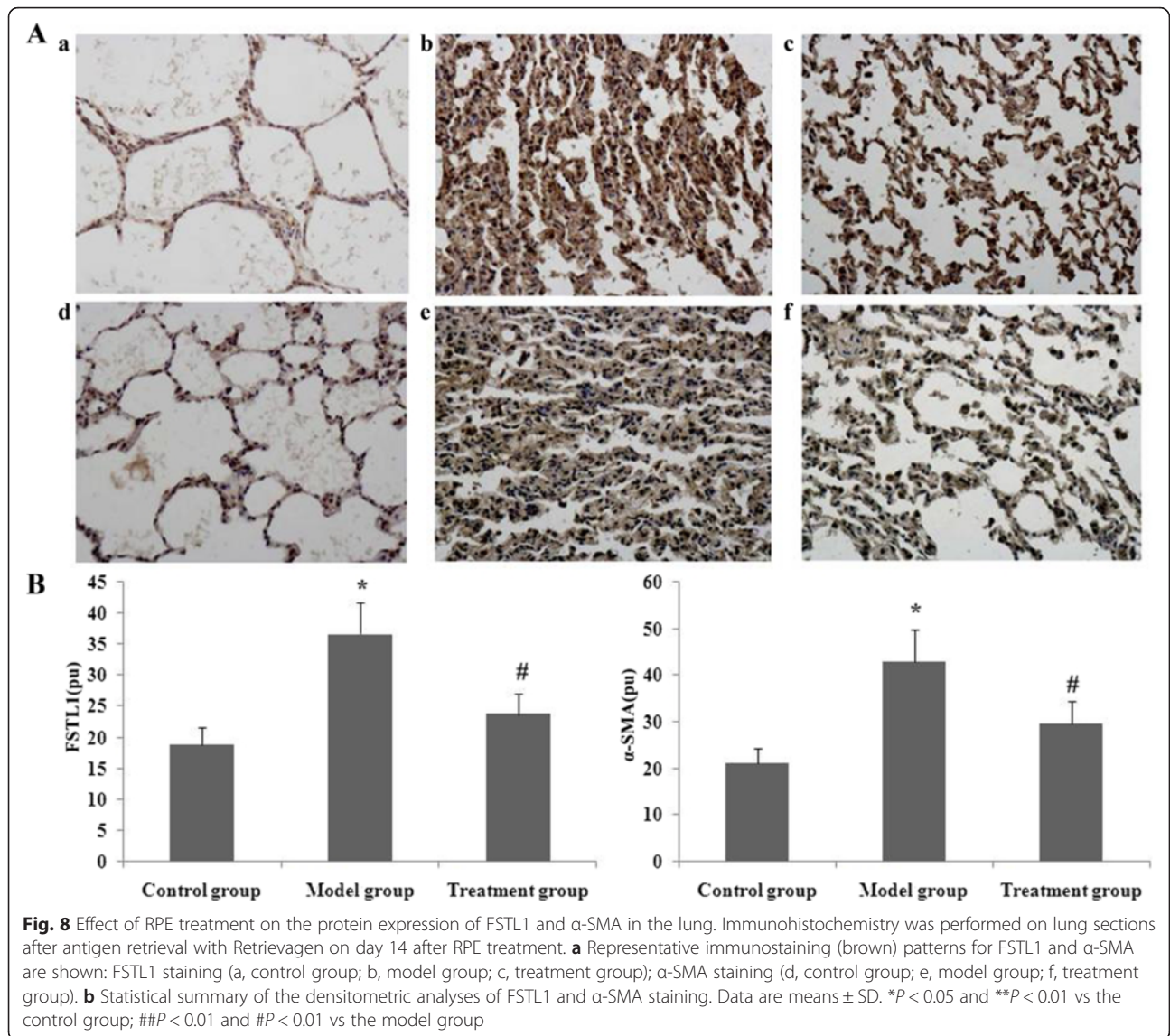
## Discussion

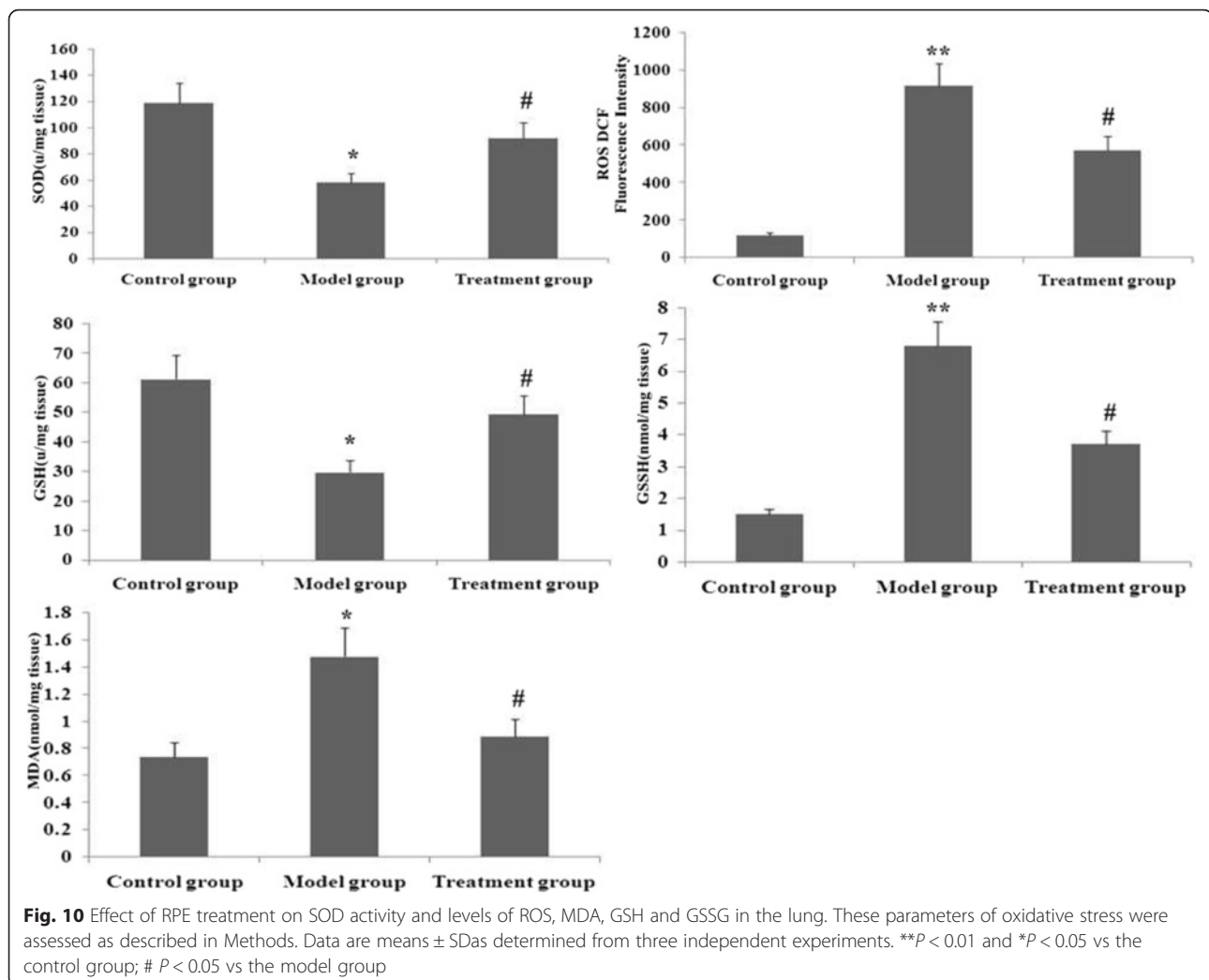
The herbicide PQ primarily accumulates in the lungs through the highly developed polyamine uptake system, leading to the generation of a superoxide radical ( $O_2^-$ ) through oxygen- and NADPH-dependent redox cycling and resulting in acute oxidative stress-related insults [27, 28]. Current treatments for PQ poisoning focus on reducing its absorption from the gastrointestinal tract and on increasing its elimination [29]. Several other interventions have been proposed but none were shown to be effective in clinical trials. The most potentially promising intervention is immunosuppressive therapy but it is not widely used because it has little supporting evidence [29, 30].

Puerarin has been reported to have protective effects related to its abilities to increase SOD activity, decrease lipid peroxidation and enhance fibrinolysis [31]. Puerarin is a scavenger of oxygen-free radicals and can prophylactically reduce the oxidative injury induced by  $H_2O_2$  and superoxide anion [32]. Recent studies indicated that puerarin inhibited oxidative stress induced by acute alcoholism [33], reduced PGE<sub>2</sub>, TNF and IL-6 production [34] and acted as an anti-inflammatory agent by blocking NF- $\kappa$ B signalling [34]. It was suggested that puerarin should be developed for chemoprevention of atherosclerosis [35]. In

our study, RPE, extracts that contain puerarin, inhibited miR-21 expression, blocked FSTL1 expression and increased HO-1 and Nrf2 protein levels in lungs from PQ-treated mice. RPE treatment also inhibited PQ-induced effects on ROS and MDA levels, downregulated gene expression of TGF- $\beta$ 1, CTGF, collagen III and collagen I and ameliorated PQ-induced pulmonary fibrosis. These results support an important role of puerarin in attenuating development of pulmonary fibrosis or protecting against pulmonary fibrosis after PQ exposure.

Because miR-21 is one of the most abundant microRNAs, it plays an important role in the pathogenesis and development of fibrosis. Previous studies indicated that miR-21 was upregulated during fibrogenesis in the heart, kidney and lung [36–38]. In addition, miR-21 was significantly upregulated during liver fibrosis of different aetiologies [39], further indicating that miR-21 is a common effector in fibrotic disease. This implies that miR-21 is an attractive potential therapeutic target against fibrosis under various pathological conditions. Upregulation of miR-21 was observed in the cardiac fibroblasts of failing hearts and treatment with an miR-21 antagonism in mouse model of cardiac hypertrophy prevented interstitial fibrosis and improved cardiac function [40]. Inhibiting miR-21 expression

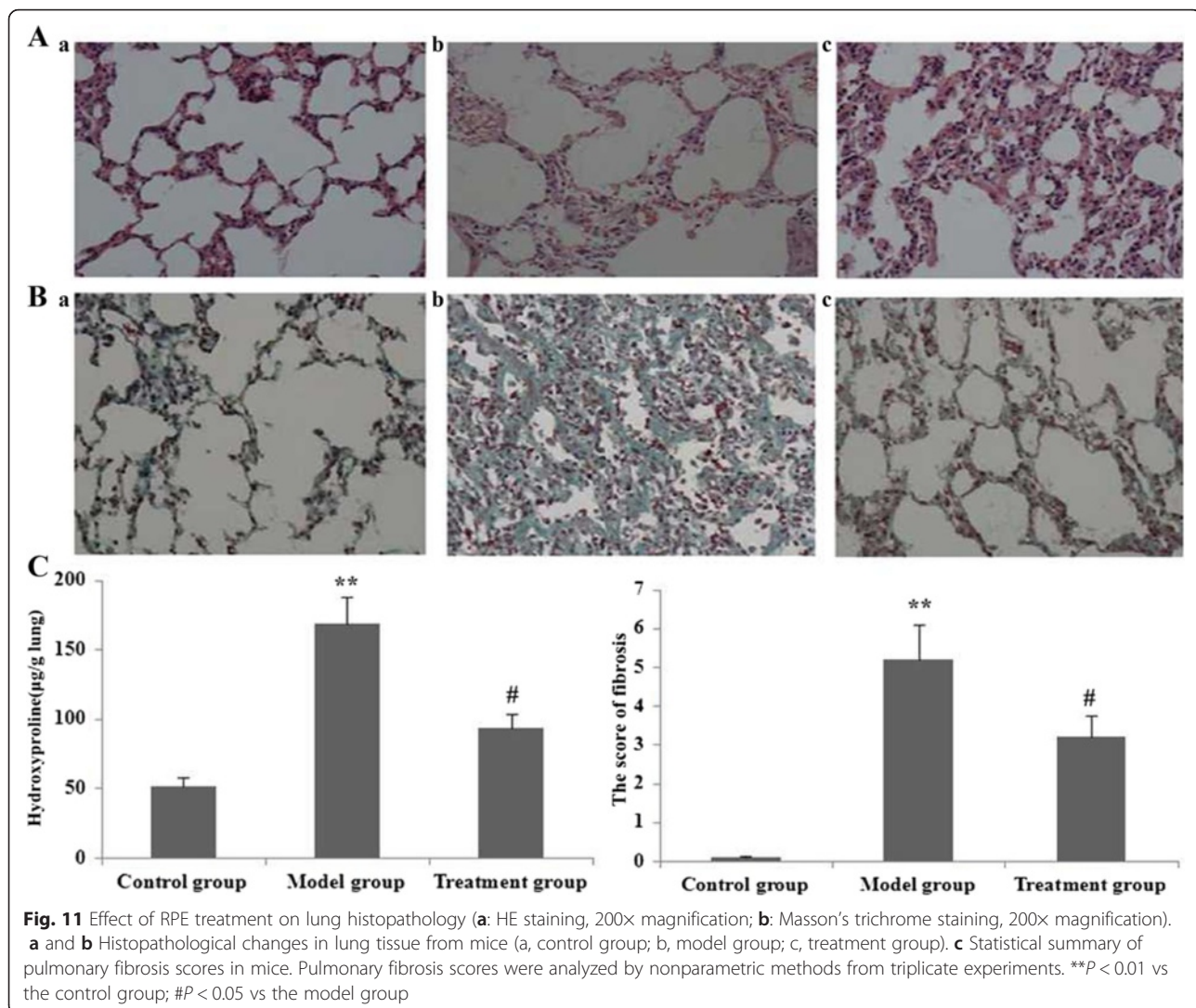




in the lung successfully ameliorated pulmonary fibrosis and it was suggested that miR-21 promoted fibrosis by targeting the anti-fibrotic protein Smad7 [41]. Smad7, as an intrinsic inhibitor of the TGF- $\beta$ /Smad2/3 pathway, competes with R-Smads for type I TGF receptors (T $\beta$ RI) and intervenes in TGF- $\beta$ /Smad2/3 signal transduction [41]. Previous studies indicated that adenovirus-mediated Smad7 overexpression in the mouse liver inhibited collagen deposition and  $\alpha$ -SMA expression in hepatic stellate cells (HSCs) [42]. In our study, PQ markedly upregulated miR-21 expression, stimulated FSTL1 expression, facilitated TGF- $\beta$ /Smad2/3 and p38MAPK signal transduction and induced pulmonary fibrosis. However, administration of RPE significantly suppressed PQ-induced miR-21 expression, blocked FSTL1 expression, decreased p-p38MAPK, NF- $\kappa$ B65, p-Smad2/3 and MMP-9 protein levels and attenuated pulmonary fibrosis.

Fstl 1 was upregulated in patients with IPF and in the bleomycin-induced model of pulmonary fibrosis [13]. In the lungs of bleomycin-treated WT mice, Fstl 1 mRNA

and FSTL1 protein levels were increased and FSTL1 immunoreactivity was evident in fibrotic areas [14]. Fstl 1 haploinsufficiency in Fstl 1 +/- mice showed a clear anti-fibrotic effect in the lungs after bleomycin treatment, as indicated by a markedly attenuated fibrotic phenotype with significantly less collagen deposition, as compared with in wild type mice [14]. These findings confirmed the critical role of FSTL1 as a profibrotic protein during progressive interstitial fibrosis [14]. In Fstl 1 +/- mice, insufficiency of FSTL1 attenuated bleomycin-induced fibrosis, with limited expansion of the myofibroblast pool because of impaired epithelial mesenchymal transition (EMT) and reduced Smad2/3, ERK and JNK phosphorylation [14]. Fstl 1 overexpression increased TGF- $\beta$ 1-induced EMT via Smad-dependent and MAPK-dependent pathways in A549 cells. In that study, selective chemical blockade of Smad2/3, ERK or JNK phosphorylation decreased expression of EMT marker proteins [14]. Our study demonstrated that Fstl 1 was upregulated through miR-21 expression after PQ challenge, resulting in increased Smad2/



3 and p38MAPK phosphorylation and progressive PQ-induced pulmonary fibrosis. RPE treatment significantly downregulated Fstl 1 expression by decreasing miR-21 expression. This decreased the expression of profibrogenic genes and directly suppressed PQ-induced fibrosis.

Smad2/3, as the primary signalling mediator, is pivotal in the TGF- $\beta$  signalling pathway. Thus, Smad2/3 mediated expression of type I collagen A1 in activated HSCs and targeted deletion of Smad2/3 prevented or halted the progression of hepatic fibrosis in animals [43]. Interestingly, in our present study, puerarin induced downregulation of Smad2/3 expression in PQ-treated mice. This likely reduced expression of profibrogenic genes and directly suppressed pulmonary fibrosis, thus protecting against miR-21-mediated injury and downregulating the major signalling transducer, Smad2/3.

CTGF is the primary downstream mediator of TGF- $\beta$ -induced fibroblast activation and its specific role in fibrotic tissue makes it a better therapeutic target than TGF- $\beta$  [44].

In our study, RPE extracts appeared to attenuate PQ-induced lung fibrosis through blocking TGF- $\beta$ 1 and CTGF expression, as a result of decreased miR-21 levels. This suggested that PQ-induced fibrosis might be mediated by miR-21-stimulated expression of the profibrotic factors TGF- $\beta$ 1 and CTGF.

PQ produces lung oxidative stress in animals [2] and humans [3]. Excessive levels of ROS damage cellular macromolecules, such as DNA, lipids and proteins, leading to oxidative stress-induced tissue injury [45]. Cellular antioxidants play a key role in removal or detoxification of ROS and are essential for preventing oxidative damage. HO-1 provides an inducible defence mechanism that can be activated ubiquitously in cells and tissues in response to noxious stimuli, conferring cellular protection against injury inflicted by such stimuli [46]. HO-1 may play an important role in protecting against PQ-induced tissue damage. Nrf2 is a redox-sensitive basic leucine zipper transcription factor of the NADPH oxidase complex that is activated by

oxidative stress and, when activated, translocates into the nucleus [47]. Nrf2 activation has been reported to play an important role in the antioxidant response element (ARE)-driven expression of several detoxifying and antioxidant enzymes, including HO-1 [48]. In this study, puerarin increased HO-1 and Nrf2 expression, suppressed ROS and MDA levels, significantly increased SOD activity and GSH levels, decreased miR-21 and Fstl 1 expression and attenuated PQ-induced pulmonary fibrosis.

TGF- $\beta$ 1 induces breakdown of collagen and other matrix proteins by enhancing generation of MMPs [48] and plasminogen activators and inhibiting expression of tissue inhibitors of metalloproteinases (TIMPs) [49]. Therefore, in addition to downregulating miR-21 and Fstl 1 expression, puerarin might interrupt the TGF- $\beta$  autocrine pathway by inhibiting MMP-9 activity and, thereby, suppress PQ-induced pulmonary fibrosis.

NF- $\kappa$ B activation increased in an animal model of lung fibrosis and blocking NF- $\kappa$ B activation suppressed lung collagen deposition and inflammation, consequently exacerbating fibrosis [50]. Several lines of evidence suggest that MAPK can participate in NF- $\kappa$ B activation in the cytoplasm as well as the modulation of its transactivation potential in the nucleus [51]. In our experiments, RPE treatment blocked the p38MAPK pathway and inhibited NF- $\kappa$ B activation by suppressing Fstl 1 expression via downregulation of miR-21 expression. This reduced lung collagen deposition and alleviated PQ-induced pulmonary fibrosis.

PQ causes destruction of the lung architecture, leading to pulmonary fibrosis, which is characterised by increased HYP levels and more collagen deposition in the lungs [52].  $\alpha$ -SMA is a marker of fibroblast activation and its presence indicates the occurrence of the fibroblast transition towards myofibroblasts [53]. The present study showed a substantially increased intensity of lung collagen staining in PQ-treated animals, reflecting the detrimental alterations associated with fibrosis. Increased HYP levels were correlated to collagen accumulation in the alveolar space. Our data also indicated that the RPE-treated mice exhibited significantly lower HYP levels and  $\alpha$ -SMA expression. The ameliorating effects of RPE on these histological alterations indicated suppression of Fstl 1 mediated effects by downregulating miR-21 expression, preventing accumulation of HYP in lungs of mice treated with PQ.

## Conclusions

The results of this study suggest a novel compensatory mechanism for the action of RPE in inhibiting lung fibrosis under its pathological induction by PQ. This mechanism involves blocking profibrotic gene and protein expression though decreasing Fstl 1 expression via downregulation of miR-21. We have demonstrated for the first time that RPE has protective, antifibrotic effects against pulmonary

fibrosis in a PQ-induced mouse model. Thus, the beneficial effects of in vivo administration of RPE on the parameters of pulmonary fibrosis described in this study support a novel potential therapeutic modality for treating PQ-induced pulmonary fibrosis and other forms of pulmonary fibrosis.

## Abbreviations

RPE: radix puerariae extract; Fstl 1: follistatin-like 1 gene; FSTL1: follistatin-like 1 protein; miR-21: microRNA-21; PQ: paraquat; CTGF: connective tissue growth factor; MMP-9: matrix metalloproteinase-9; ECM: extracellularmatrix; TIMPs: tissue inhibitors of metalloproteinases; Nrf2: nuclear factor erythroid 2p45-related factor-2; MAPKs: mitogen-activated protein kinases; NF- $\kappa$ B: nuclear factor kappa;  $\alpha$ -SMA: alpha-smooth muscle actin; ROS: reactive oxygen species; HO-1: heme oxygenase-1; SOD: superoxide dismutase; TGF- $\beta$ : transforming growth factor- $\beta$ ; MDA: malondialdehyde; GSH: reduced glutathione; GSSH: oxidised glutathione; HSCs: hepatic stellate cells.

## Competing interests

The authors declare that no competing interest exists.

## Authors' contributions

LM and SM conceived and designed the experiments. LM, ZY and CM performed the experiments. LM and ZL analysed the data. LM, ZY and ZL contributed to reagents, materials and analysis tools. LM wrote the paper. All authors contributed to and have read and approved the final manuscript.

## Acknowledgements

The authors thank Prof. Qin-qin Huang and Prof. Lan-fang Qin for technical advice.

## Author details

<sup>1</sup>Department of Emergency, the First Affiliated Hospital of Kunming Medical University, 295 Xichang Road, Wu Hua District, Kunming 650032, China.

<sup>2</sup>Emergency Intensive Care Unit, the Second Affiliated Hospital of Kunming Medical University, Kunming 650106, China.

Received: 14 May 2015 Accepted: 8 January 2016

Published online: 12 January 2016

## References

- Cristovao AC, Choi DH, Baltazar G, Beal MF, Kim YS. The role of NADPH oxidase 1-derived reactive oxygen species in paraquat-mediated dopaminergic cell death. *Antioxid Redox Signal*. 2009;11:2105–8.
- Suntres ZE. Role of antioxidants in paraquat toxicity. *Toxicology*. 2002;180:65–77.
- Qian J, Ye Y, Lv L, Zhu C, Ye S. FTY720 attenuates paraquat-induced lung injury in mice. *Int Immunopharmacol*. 2014;21:426–31.
- Chang X, Shao C, Wu Q, Wu Q, Huang M, Zhou Z. Pyrrolidine dithiocarbamate attenuates paraquat-induced lung injury in rats. *Biomed Biotechnol*. 2009;6:1948:7.
- Keung WM. Biochemical studies of a new class of alcohol dehydrogenase inhibitors from Radix puerariae. *Alcohol Clin Exp Res*. 1993;17:1254–60.
- Benlhabib E, Baker JI, Keyler DE, Singh AK. Effects of purified puerarin on voluntary alcohol intake and alcohol withdrawal symptoms in P rats receiving free access to water and alcohol. *J Med Food*. 2004;7:180–6.
- Choo MK, Park EK, Yoon HK, Kim DH. Antithrombotic and antiallergic activities of daidzein, a metabolite of puerarin and daidzin produced by human intestinal microflora. *Biol Pharm Bull*. 2002;25:1328–32.
- Guerra MC, Speroni E, Broccoli M, Cangini M, Pasini P, Minghetti A, et al. Comparison between chinese medical herb Pueraria lobata crude extract and its main isoflavone puerarin antioxidant properties and effects on rat liver CYP-catalysed drug metabolism. *Life Sci*. 2000;67:2997–3006.
- Han RM, Tian YX, Becker EM, Andersen ML, Zhang JP, Skibsted LH. Puerarin and conjugate bases as radical scavengers and antioxidants: molecular mechanism and synergism with betacarotene. *J Agric Food Chem*. 2007;55:2384–91.
- Jazbutyte V, Thum T. MicroRNA-21: from cancer to cardiovascular disease. *Curr Drug Targets*. 2010;11:926–35.

11. Zhong X, Chung AC, Chen HY, Meng XM, Lan HY. Smad3-mediated upregulation of miR-21 promotes renal fibrosis. *J Am Soc Nephrol*. 2011;22:1668–81.
12. Yang G, Yang L, Wang W, Wang J, Wang J, Xu Z. Discovery and validation of extracellular/circulating microRNAs during idiopathic pulmonary fibrosis/disease progression. *Gene*. 2015;562:138–144.
13. Chaly Y, Hostager B, Smith S, Hirsch R. Follistatin-like protein 1 and its role in inflammation and inflammatory diseases. *Immunol Res*. 2014;59:266–72.
14. Dong Y, Geng Y, Li L, Li X, Yan X, Fang Y, et al. Blocking follistatin-like 1 attenuates bleomycin-induced pulmonary fibrosis in mice. *J Exp Med*. 2015; 212:235–52.
15. Wang Q, Usinger W, Nichols B, Gray J, Xu L, Seeley TW, et al. Cooperative interaction of CTGF and TGF- $\beta$  in animal models of fibrotic disease. *Fibrogenesis Tissue Repair*. 2011;4:4.
16. Lipson KE, Wong C, Teng Y, Spong S. CTGF is a central mediator of tissue remodeling and fibrosis and its inhibition can reverse the process of fibrosis. *Fibrogenesis Tissue Repair*. 2012;5:S24.
17. Walters DM, Cho HY, Kleeberger SR. Oxidative stress and antioxidants in the pathogenesis of pulmonary fibrosis: a potential role for Nrf2. *Antioxid Redox Signa*. 2008;10:321–32.
18. Xu X, Krieger AJ, Liu Y, Usa K, Mladinov D, Liu H, et al. Delayed ischemic preconditioning contributes to renal protection by upregulation of miR-21. *Kidney Int*. 2012;82:1167–75.
19. Zhou X, Li YJ, Gao SY, Wang XZ, Wang PY, Yan YF, et al. Sulindac has strong antifibrotic effects by suppressing STAT3-related miR-21. *J Cell Mol Med*. 2015;19:1103–1113.
20. Zhu J, Nguyen D, Ouyang H, Zhang XH, Chen XM, Zhang K. Inhibition of RhoA/Rho-kinase pathway suppresses the expression of extracellular matrix-induced by CTGF or TGF- $\beta$  in ARPE-19. *Int J Ophthalmol*. 2013;6:8–14.
21. Chang L, Karin M. Mammalian MAP kinase signalling cascades. *Nature*. 2001; 410:37–40.
22. Yamamoto K, Hamada H, Shinkai H, Kohno Y, Koseki H, Aoe T. The KDEL receptor modulates the endoplasmic reticulum stress response through mitogen-activated protein kinase signaling cascades. *J Biol Chem*. 2003;278: 34525–32.
23. Mukhopadhyay P, Rajesh M, Haskó G, Hawkins BJ, Madesh M, Pacher P. Simultaneous detection of apoptosis and mitochondrial superoxide production in live cells by flow cytometry and confocal microscopy. *Nat Protoc*. 2007;2:2295–301.
24. Kakkar P, Das B, Viswanathan PN. A modified spectrophotometric assay of superoxide dismutase. *Indian J Biochem Biophys*. 1984;21:130–2.
25. Edwards CA, O'Brien Jr WD. Modified assay for determination of hydroxyproline in a tissue hydrolyzate. *Clin Chim Acta*. 1980;104:161–7.
26. Ashcroft T, Simpson JM, Timbrell V. Simple method of estimating severity of pulmonary fibrosis on a numerical scale. *J Clin Pathol*. 1988;41:467–70.
27. Bus JS, Aust SD, Gibson JE. Superoxide- and singlet oxygen-catalyzed lipid peroxidation as a possible mechanism for paraquat (methyl viologen) toxicity. *Biochem Biophys Res Commun*. 1974;58:749–55.
28. Bus JS, Gibson JE. Paraquat: model for oxidant-initiated toxicity. *Environ Health Perspect*. 1984;55:37–46.
29. Eddleston M, Wilks MF, Buckley NA. Prospects for treatment of paraquat-induced lung fibrosis with immunosuppressive drugs and the need for better prediction of outcome: a systematic review. *QJM*. 2003;96:809–24.
30. Bismuth C, Hall AH, Baud FJ. Pulmonary dysfunction in survivors of acute paraquat poisoning. *Vet Hum Toxicol*. 1996;38:220–2.
31. Gao Q, Yang B, Ye ZG, Wang J, Bruce IC, Xia F. Opening the calcium-activated potassium channel participates in the cardioprotective effect of puerarin. *Eur J Pharmacol*. 2007;574:179–84.
32. Zhu QL, He AX, Lu XR. Effects of puerarin on the scavenge of oxygen free radicals and the antagonism against oxidative injury. *Pharm J Clin PLA*. 2001;17:1–3.
33. Zhao M, Du YQ, Yuan L, Wang NN. Protective effect of puerarin on acute alcoholic liver injury. *Am J Chin Med*. 2010;38:241–9.
34. Xu C, Li G, Gao Y, Liu S, Lin J, Zhang J, et al. Effect of puerarin on P2X3 receptor involved in hyperalgesia after burn injury in the rat. *Brain Res Bull*. 2009;80:341–6.
35. Yang X, Hu W, Zhang Q, Wang Y, Sun L. Puerarin inhibits C-reactive protein expression via suppression of nuclear factor kappaB activation in lipopolysaccharide-induced peripheral blood mononuclear cells of patients with stable angina pectoris. *Basic Clin Pharmacol Toxicol*. 2010;107:637–42.
36. Patel V, Noureddine L. MicroRNAs and fibrosis. *Curr Opin Nephrol Hypertens*. 2012;21:410–6.
37. He Y, Huang C, Li J. miR-21 is a critical therapeutic target for renal fibrosis. *Cell Biochem Biophys*. 2014;68:635–6.
38. Huang Y, He Y, Li J. MicroRNA-21: a central regulator of fibrotic diseases via various targets. *Curr Pharm Des*. 2015;21:2236–2242.
39. Wei J, Feng L, Li Z, Xu G, Fan X. MicroRNA-21 activates hepatic stellate cells via PTEN/Akt signaling. *Biomed Pharmacother*. 2013;67:387–92.
40. Thum T, Gross C, Fiedler J, Fischer T, Kissler S, Bussen M, et al. MicroRNA-21 contributes to myocardial disease by stimulating MAP kinase signalling in fibroblasts. *Nature*. 2008;456:980–4.
41. Liu G, Friggeri A, Yang Y, Milosevic J, Ding Q, Thannickal VJ, et al. miR-21 mediates fibrogenic activation of pulmonary fibroblasts and lung fibrosis. *J Exp Med*. 2010;207:1589–97.
42. Cook NL, Pereira TN, Lewindon PJ, Shepherd RW, Ramm GA. Circulating MicroRNAs as Noninvasive Diagnostic Biomarkers of Liver Disease in Children With Cystic Fibrosis. *J Pediatr Gastroenterol Nutr*. 2015;60:247–54.
43. Yang Y, Kim B, Park YK, Koo SI, Lee JY. Astaxanthin prevents TGF $\beta$ 1-induced pro-fibrogenic gene expression by inhibiting Smad3 activation in hepatic stellate cells. *Biochim Biophys Acta*. 2015;1850:178–85.
44. Brigstock DR. The CCN family: a new stimulus package. *J Endocrinol*. 2003; 178:169–75.
45. Melegari SP, Perreault F, Costa RH, Popovic R, Matias WG. Evaluation of toxicity and oxidative stress induced by copper oxide nanoparticles in the green alga *Chlamydomonas reinhardtii*. *Aquat Toxicol*. 2013;142–143:431–40.
46. Ryter SW, Alam J, Choi AM. Heme oxygenase-1/carbon monoxide: from basic science to therapeutic applications. *Physiol Rev*. 2006;86:583–650.
47. Jhang KA, Lee EO, Kim HS, Chong YH. Norepinephrine provides short-term neuroprotection against A $\beta$ 1-42 by reducing oxidative stress independent of Nrf2 activation. *Neurobiol Aging*. 2014;35:2465–73.
48. Rushworth SA, MacEwan DJ, O'Connell MA. Lipopolysaccharide-induced expression of NAD(P)H:quinone oxidoreductase 1 and heme oxygenase-1 protects against excessive inflammatory responses in human monocytes. *J Immunol*. 2008;181:6730–7.
49. Singh MK, Bhattacharya D, Chaudhuri S, Acharya S, Kumar P, Santra P, et al. T11TS inhibits glioma angiogenesis by modulation of MMPs, TIMPs, with related integrin  $\alpha$ v and TGF- $\beta$ 1 expressions. *Tumour Biol*. 2014;35:2231–46.
50. El-Khouly D, El-Bakly WM, Awad AS, El-Mesallamy HO, El-Demerdash E. Thymoquinone blocks lung injury and fibrosis by attenuating bleomycin-induced oxidative stress and activation of nuclear factor Kappa-B in rats. *Toxicology*. 2012; 302:106–13.
51. Liu MW, Su MX, Zhang W, Wang YQ, Chen M, Wang L, et al. Protective effect of Xuebijing injection on paraquat-induced pulmonary injury via down-regulating the expression of p38 MAPK in rats. *BMC Complement Altern Med*. 2014;14:498.
52. Azambuja E, Fleck JF, Batista RG, Menna Barreto SS. Bleomycin lung toxicity: Who are the patients with increased risk? *Pulm Pharmacol Ther*. 2005;18:363–6.
53. Chia HN, Vigen M, Kasko AM. Effect of substrate stiffness on pulmonary fibroblast activation by TGF- $\beta$ . *Acta Biomater*. 2012;8:2602–11.

Submit your next manuscript to BioMed Central and we will help you at every step:

- We accept pre-submission inquiries
- Our selector tool helps you to find the most relevant journal
- We provide round the clock customer support
- Convenient online submission
- Thorough peer review
- Inclusion in PubMed and all major indexing services
- Maximum visibility for your research

Submit your manuscript at  
[www.biomedcentral.com/submit](http://www.biomedcentral.com/submit)

